CETRA2026 27-30 May 2026, Bol, Island Brač, Croatia
9th International Conference on Road and Rail Infrastructure

SIMULATING EFFECT OF HIGH-SPEED RAIL ON UNDERGROUND TUNNEL THROUGH SOIL STRUCTURE INTERACTION ANALYSIS AND NUMERICAL MODELLING USING PLAXIS 3D

Manish V Shah[1], **Neha Tiwari**[2], **Priti J Mehta**[2]
[1]*Applied Mechanics Department, Government Engineering College, Bharuch, Gujarat, India*
[2]*Applied Mechanics Department, L.D. College of Engineering, Ahmedabad, Gujarat, India*

Abstract

Ballastless high-speed railway tunnels are subjected to complex dynamic soil–structure interaction (SSI) effects due to repeated moving train loads, which can significantly influence tunnel stability and long-term service performance. Accurate prediction of tunnel deformation and stress redistribution under such loading conditions is therefore essential for safe and economical design. This study presents a three-dimensional numerical investigation of a circular underground tunnel subjected to both static and moving high-speed train loads under hydrostatic pressure conditions. Finite element simulations were conducted using PLAXIS 3D, considering realistic soil stratification, tunnel lining properties, and train loading models based on feasibility guidelines. The numerical framework integrates soil–structure interaction mechanisms with analytical formulations to evaluate tunnel deformation, stress distribution, and subgrade stiffness. Results indicate that dynamic loading significantly amplifies tunnel displacement compared to static conditions, with maximum vertical displacements of 13.36 mm and 10.62 mm, respectively. The calculated modulus of subgrade reaction decreases under dynamic loading, highlighting the importance of displacement-dependent soil stiffness in high-speed rail tunnel design.

Keywords: soil structure interaction, high speed rail, finite element modelling, dynamic analysis

1 Introduction

High-speed railway tunnels are subjected to complex dynamic loading conditions arising from repeated train movements, which induce significant soil–structure interaction (SSI) effects and influence tunnel stability, serviceability, and long-term structural performance. The increasing operational speeds and axle loads of modern rail systems amplify ground-borne vibrations and cyclic stresses within the surrounding soil, making accurate prediction of tunnel deformation and stress redistribution essential for safe and economical design. In particular, the presence of layered soil profiles and groundwater conditions further complicates tunnel behavior, necessitating advanced numerical modelling techniques capable of capturing three-dimensional dynamic responses. Extensive research has been conducted to investigate the dynamic behavior of tunnels and surrounding soils under train-induced vibrations using analytical, experimental, and numerical approaches. Analytical solutions for stress distribution around circular openings under plane strain conditions were first proposed by Kirsch, providing theoretical insight into radial, tangential, and shear stress development around tunnels. Numerical studies have examined acceleration and displacement responses of soils surrounding subway tunnels under dynamic loading [7], while dynamic model tests

DOI: https://doi.org/10.5592/CO/CETRA.2026.1938

have explored the effects of train speed on stress propagation and tunnel invert response [8]. Three-dimensional finite element models incorporating train–tunnel–soil interaction have further enabled detailed investigation of vibration transmission, soil displacement, and strain behavior [9-11]. Cyclic train loading has been shown to induce permanent deformation and progressive accumulation of plastic strain in cohesive soils, significantly contributing to long-term tunnel settlement [12-18]. Field measurements and numerical investigations have demonstrated that soil response under repeated train passages is governed by soil type, stress state, loading frequency, and groundwater conditions [19-24]. While several studies have adopted elastic or viscoelastic soil models to evaluate vibration propagation, comparatively fewer investigations have incorporated three-dimensional elastoplastic modelling combined with hydrostatic pressure effects and realistic high-speed train loading scenarios. Furthermore, most existing studies have primarily focused on vibration propagation and its impact on nearby structures, whereas quantitative evaluation of tunnel settlement and stress redistribution under high-speed rail loading remains relatively limited. The combined influence of moving loads, layered soil stratigraphy, groundwater pressure, and tunnel lining stiffness on tunnel performance requires further systematic investigation. Advanced three-dimensional finite element modelling provides an effective framework for addressing these complexities and capturing realistic soil–structure interaction mechanisms. In this context, the present study aims to investigate the static and dynamic response of a circular high-speed rail tunnel under hydrostatic pressure conditions using three-dimensional finite element modelling in PLAXIS 3D. The analysis incorporates realistic soil layering, elastoplastic soil constitutive behavior, tunnel lining properties, and moving train loads defined according to [1-6] tunnel deformation, stress redistribution, velocity response, and subgrade stiffness characteristics under both static and moving loading conditions. The outcomes provide valuable insight into tunnel performance in layered soil environments and contribute to the development of reliable design strategies for high-speed railway tunnel infrastructure.

2 Numerical modelling and establishment of parameters

2.1 Tunnel geometry simulation and software input parameters

A three-dimensional finite element model was developed using PLAXIS 3D to simulate the dynamic soil–structure interaction behavior of a circular underground tunnel subjected to static and moving high-speed train loads [1-6]. A three-dimensional modelling approach was adopted to realistically capture the spatial variation of stress redistribution, wave propagation, and tunnel deformation, which cannot be adequately represented using simplified two-dimensional or plane strain assumptions under dynamic loading conditions. The numerical domain extends 40 m in the longitudinal direction, 34.7 m in the transverse direction, and 34.5 m in the vertical direction, providing sufficient spatial extent to minimize boundary effects and ensure accurate simulation of stress wave propagation. The tunnel is modelled as a circular structure with an outer diameter of 8.5 m, an inner diameter of 8.0 m, and a lining thickness of 0.25 m. The tunnel crown is located at a depth of 13.25 m below ground surface, representing typical shallow-buried urban tunnelling conditions as shown in figure 1. To avoid spurious stress wave reflections during dynamic analysis, viscous absorbing boundaries were applied along the lateral faces of the model, while the base of the domain was fully fixed in both vertical and horizontal directions. The ground surface was kept free, allowing natural deformation under applied loads. This boundary configuration ensures numerical stability and replicates realistic far-field ground behavior under dynamic excitation. The tunnel lining was modelled as a linear elastic material, as structural deformation of the lining was assumed to remain within elastic limits under the applied loading conditions.

The surrounding soil mass was modelled using an elastoplastic Mohr–Coulomb constitutive model, which captures essential soil strength and deformation characteristics while maintaining computational efficiency for dynamic analysis. Segmental joints in the tunnel lining were neglected, and the lining was idealized as a continuous homogeneous ring to focus on the global tunnel–soil interaction response.

2.2 Soil stratigraphy and material properties

Subsurface conditions were defined based on borehole investigation data, identifying multiple soil layers comprising sand, clay, silt, and gravelly soils. The soil stratification reflects typical alluvial soil profiles encountered in urban underground construction. Each soil layer was assigned appropriate mechanical and hydraulic properties, including unit weight, cohesion, friction angle, Young's modulus, and Poisson's ratio, as summarized in table 1. The Mohr–Coulomb soil model was selected due to its widespread application in tunnel engineering practice and its ability to capture nonlinear soil behavior under combined static and cyclic loading. This model allows simulation of plastic yielding and permanent deformation accumulation, which are critical for evaluating tunnel settlement and long-term serviceability under repeated train passages. The tunnel lining and track components were assigned linear elastic properties consistent with standard reinforced concrete and rail material specifications. The railway track system consisted of rails, rail pads, sleepers, slab track, and subsoil. Rails and sleepers were modelled as beam elements to realistically represent their flexural stiffness and load distribution characteristics. Rail pads were simulated using node-to-node elastic connections, enabling appropriate representation of load transmission and vibration damping between the rail and sleeper system. The mechanical properties assigned to these components are presented in table 2.

Table 1 Model material parameters of numerical calculation

No.	Soil layers	γ_{sat} [kN/m³]	γ_{unsat} [kN/m³]	υ	φ' [°]	c' [kN/m²]	Ψ	E' [kN/m²]
1	Upper sand	20	17	0.3	31	1	0	13000
2	Clay	18	16	0.35	25	5	0	10000
3	Dense sand	20	17	0.3	31	1	0	75000
4	Concrete	-	27	0.1	-	-	-	31000000
5	Protective layer	23	22	0.25	40	30	15	55000
6	Clay of medium plasticity	19.6	15.8	0.25	23	11	0	30000
7	Silty gravel	17.4	14.6	0.25	25	9	0	32000
8	Silt of low plasticity	20.52	17.81	0.25	25	9	0	48000

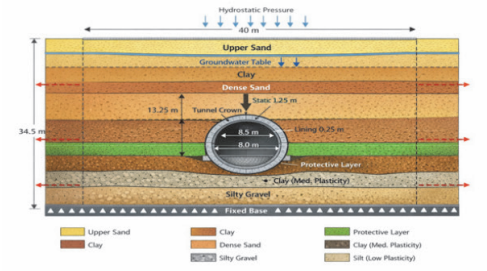

Figure 1 Cross-sectional view of the high-speed rail tunnel

Table 2 Properties adapted in Plaxis 3D for rail and sleeper

Parameter	Unit	Rail	Sleeper
Cross section area (A)	m^2	7.7×10^{-3}	5.13×10^{-2}
Unit weight (Y)	kN/m^3	78	25
Young's modulus (E)	kN/m^3	200×10^6	36×10^6
Moment of inertia around the second axis (I3)	m^4	3.05×10^{-5}	0.025
Moment of inertia around the third axis (I2)	m^4	5.13×10^{-6}	2.45×10^{-4}

2.3 Loading scheme and simulation of train movement

The dynamic loading induced by high-speed rail traffic was simulated using a moving load model based on the ICE German rail car configuration as shown in table 3, which represents a widely adopted reference model in railway dynamic studies. The total length of the vehicle is 21.7 m as shown in figure 2, and the axle configuration was used to define the spatial and temporal distribution of dynamic loads along the rails.

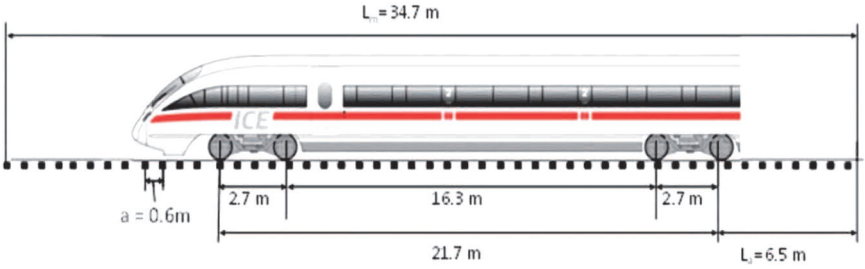

Figure 2 Basic dimensions of ICE German rail car (Ahmed Elgamal, 2020)

The computational model length was extended to 34.7 m, incorporating additional buffer zones at both ends to prevent artificial stress wave reflections and ensure complete passage of the moving load through the numerical domain. Train speed and axle spacing were incorporated to generate time-dependent load functions applied sequentially at rail–sleeper contact points. This approach enables realistic simulation of dynamic excitation induced by moving trains. Two loading scenarios were considered based on tunnel under dry condition (TUDC) and tunnel under hydrostatic pressure condition (TUHP):

- static loading condition as shown in figure 4a, representing stationary axle loads of 250 kN per axle (125 kN per wheel) as shown in figure 3, in accordance with UIC 71 specifications
- moving loading condition as shown in figure 4b, representing dynamic passage of the same axle loads along the track at operational speed, consistent with UIC 71 and Eurocode 1 recommendations.

The applied loading scheme captures the transient nature of dynamic stresses transmitted from the rail–track system to the tunnel lining and surrounding soil. Hydrostatic pressure corresponding to the groundwater table was incorporated in the analysis to evaluate tunnel response under saturated conditions.

Table 3 Basic dimensions of ICE German rail car

Distance between the first and the last wagon axles [m]	L	21.7
Additional length for model [m]	$L_a = 0.3L$	6.5
Total additional length (right and left) [m]	$L_{a,\,total} = 2 \cdot 0.3L$	13.0
Model length [m]	$L_m = L+0.6L$	34.7
Sleepers distance [m]	a	0.6
Dynamic loads distance [m]	a/2	0.3
Number of dynamic loads for one rail [-]	$(2L_m)/a$	117
Number of dynamic loads for whole model (two rails) [-]	$(4L_m)/a$	234

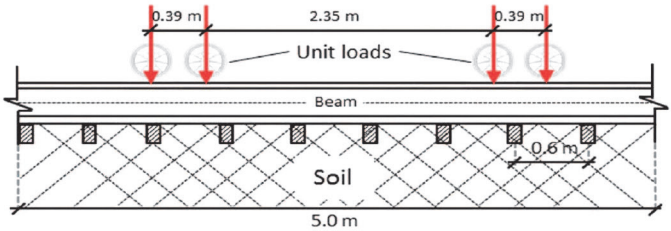

Figure 3 Loads acting on rail

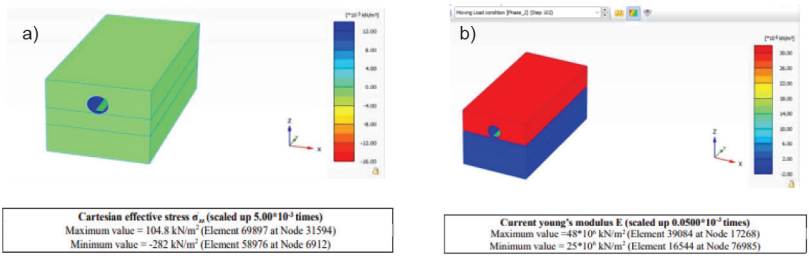

Figure 4 Tunnel under static (a) and moving (b) load condition and lateral displacement; the magnitude of each load for different cases was applied as per European codes

2.4 Analytical stress evaluation and role of kirsch equations

To provide a theoretical reference framework for stress redistribution around circular tunnel openings, classical Kirsch analytical solutions were employed. These closed-form expressions describe radial, tangential, and shear stresses around a circular cavity subjected to in-situ stresses under plane strain conditions. In the present study, Kirsch equations were not used as direct design tools but were adopted as a benchmark to qualitatively interpret numerical stress contours and validate general trends of stress concentration around the tunnel periphery obtained from PLAXIS 3D simulations. This combined analytical–numerical approach enhances confidence in the reliability of numerical predictions and facilitates improved understanding of tunnel stress behavior under complex loading conditions.

2.5 Hybrid modelling approach and determination of subgrade reaction modulus

A hybrid modelling approach was adopted in this study, combining three-dimensional finite element analysis with analytical soil mechanics formulations to evaluate tunnel response and soil stiffness characteristics.

While PLAXIS 3D was employed to compute detailed distributions of stress, displacement, and velocity within the soil–tunnel system, empirical analytical relations were utilized to estimate the modulus of subgrade reaction. The modulus of subgrade reaction (k) is not an intrinsic soil property but a response parameter that reflects the interaction between soil stiffness and structural deformation. Using settlement values obtained from finite element simulations, the modulus of subgrade reaction was calculated based on Boussinesq's elastic half-space theory, expressed as:

$$k = q/\Delta z \tag{1}$$

where q is the applied pressure and Δz is the resulting vertical displacement. This approach enables quantification of displacement-dependent soil stiffness and provides practical input for structural design and performance evaluation of tunnel systems. The hybrid modelling framework thus integrates detailed numerical simulation of soil–structure interaction with analytical evaluation of stiffness parameters, offering a comprehensive methodology for tunnel design under high-speed railway loading. The results are represented in table 4.

Modulus of Subgrade reaction (K) [kN/m³]	
Static condition	11770.2
Moving condition	9356.3

Table 4 Results of Modulus of Subgrade Reaction

3 Results

This section presents numerical results for the high-speed rail tunnel under static and moving-load conditions using PLAXIS 3D. Key parameters such as displacement, stress, and subgrade stiffness are evaluated to understand tunnel behavior.

3.1 Tunnel displacement

The displacement results under static and moving conditions are summarized in table 5. Under static loading, the total displacement |u| ranges up to 12.14 mm, while vertical displacement (uz) reaches –71.02 mm near the tunnel crown and invert. These negative values indicate localized settlement due to soil consolidation. Under moving loads, displacement increases, with maximum |u| reaching 18 mm. The vertical displacement varies between –31.63 mm and 13.36 mm, showing the effect of dynamic loading. However, all values remain within the permissible limit of 25 mm. Static loading results in localized deformation near the crown, whereas moving loads produce more distributed deformation along the tunnel.

Table 5 Summary of Tunnel Displacement

Condition	**Max |u|** [mm]	**Min uz**[mm]	**Min uz** [mm]
Static	12.14 (n:1644)	-71.02 (n:1643)	10.62 (n:15801)
Moving	18 (n:1644)	-31.63 (n:1643)	13.36 (n:15801)

3.2 Stress distribution

The vertical effective stress (σ › zz) and maximum shear stress (T_{max}) under both loading conditions are shown in table 6. The stress distribution is evaluated in terms of vertical effective stress (σ › zz) and maximum shear stress (T_{max}). Under static conditions, σ›zz varies from –7,260 kPa to 1,298 kPa, with tensile stresses observed in shallow layers and compressive stresses near the tunnel invert. Under moving loads, the stress range reduces significantly, indicating redistribution due to dynamic effects. The maximum shear stress occurs at the crown and invert, identifying critical zones. However, stress levels remain within safe limits for the tunnel lining.

Table 6 Summary of tunnel stresses

Condition	**Max σ › zz** [kPa]	**Min σ › zz** [kPa]	**Max T_{max}** [kPa]
Static	1,298	-7,260	14.30
Moving	90.75	-40.67	15.10

Note: Values reflect the highest local stresses in the model; tensile stresses are considered within acceptable safety margins due to concrete lining and surrounding soil support

3.3 Modulus of subgrade reaction (k)

The modulus of subgrade reaction (k) is calculated using displacement results. The analysis shows that k decreases with increasing displacement, indicating nonlinear soil behavior. This reduction in stiffness affects internal forces in the tunnel lining, highlighting the importance of accurate soil modelling in design.

3.4 Dynamic response under moving loads

Moving loads generate transient displacement and velocity responses, with vertical velocity reaching 0.1166 m/s. The tunnel under hydrostatic pressure shows more uniform stress distribution, improving resistance to lateral deformation. In contrast, the dry tunnel condition provides better vibration damping, which can enhance track performance and passenger comfort.

3.5 Key observations

The results show that displacement and stress patterns are influenced by soil properties and loading conditions. Load transfer is generally uniform, with some localized critical zones. Overall, the numerical model effectively captures soil–structure interaction and provides reliable results for tunnel analysis.

4 Conclusion

The study evaluates the behavior of a high-speed rail tunnel under static and dynamic loading using PLAXIS 3D. The results show that the tunnel remains stable under both loading conditions, with displacements and stresses within permissible limits. Static loads create localized stress concentrations, while moving loads lead to more uniform stress distribution. The modulus of subgrade reaction decreases with increasing displacement, indicating nonlinear soil behavior.

This significantly affects tunnel performance and should be considered in design. From a design perspective, hydrostatic conditions improve stress distribution, whereas dry conditions provide better vibration control. Therefore, tunnel design should consider both geotechnical and operational factors. Overall, the study highlights the importance of combining static and dynamic analysis. Future work should include field validation to improve reliability.

References

[1] International Union of Railways (UIC): UIC 71 – Loads to be Considered in Railway Bridge Design, Paris, France

[2] European Committee for Standardization: Eurocode 7: Geotechnical Design – Part 1: General Rules, EN 1997-1, Brussels, 2004.

[3] European Committee for Standardization: Eurocode 8: Design of Structures for Earthquake Resistance – Part 5: Foundations, Retaining Structures and Geotechnical Aspects, EN 1998-5, Brussels, 2004.

[4] Indian Roads Congress: IRC SP:087 – Manual of Specifications and Standards for Six-Laning of Highways, 2nd Rev., New Delhi, India, 2019.

[5] Bureau of Indian Standards: IS 5878 (Part 3): Code of Practice for Construction of Tunnels, New Delhi, India, 1972., reaffirmed 2020.

[6] National High-Speed Rail Corporation Limited (NHSRCL): High-Speed Rail Feasibility Study and Design Guidelines, India, 2016.

[7] He, C., Ren, F., Sun, J.: Dynamic response of tunnel structures subjected to high-speed train loading, Soil Dynamics and Earthquake Engineering, 70 (2015), pp. 1–14, DOI: 10.1016/j.soildyn.2014.11.010

[8] Huang, H., Han, J., Wang, Y.: Dynamic analysis of underground tunnel structures under moving train loads, Tunnelling and Underground Space Technology, 45 (2015), pp. 1–10, DOI: 10.1016/j.tust.2014.09.006

[9] Pan, Y., Chen, Z., Liu, H.: Dynamic soil–structure interaction analysis of tunnels under high-speed railway loading, Soil Dynamics and Earthquake Engineering, 132 (2020), 106080, DOI: 10.1016/j.soildyn.2020.106080

[10] Yang, Y., Xu, J., Li, C.: Numerical modeling of train-induced vibration effects on underground structures, Engineering Structures, 231 (2021), 111752, DOI: 10.1016/j.engstruct.2020.111752

[11] Jin, Y., Zhang, X., Wang, H.: Dynamic response of tunnel lining subjected to high-speed railway loads, Tunnelling and Underground Space Technology, 120 (2022), 104281, DOI: 10.1016/j.tust.2021.104281

[12] Brown, S.F., Lashine, A.K.F., Hyde, A.F.L.: Repeated load triaxial testing of a silty clay, Géotechnique, 25 (1975) 1, pp. 95–114, DOI: 10.1680/geot.1975.25.1.95

[13] Sangrey, D.A., Henkel, D.J.: Stress-strain and strength characteristics of cohesive soils, Journal of Soil Mechanics and Foundations Division, ASCE, 95 (1969) SM4, pp. 1045–1070

[14] Lee, K.L., Focht, J.A.: Strength of clay subjected to repeated loading, Journal of Geotechnical Engineering Division, ASCE, 102 (1976) GT11, pp. 1097–1110

[15] Yasuhara, K., Murakami, S., Ue, T.: Post cyclic behavior of saturated clay, Soils and Foundations, 22 (1982) 4, pp. 1–15, DOI: 10.3208/sandf1972.22.4_1

[16] Huang, H., Han, J.: Dynamic characteristics of soft clay under cyclic loading, Soil Dynamics and Earthquake Engineering, 29 (2009) 4, pp. 748–755, DOI: 10.1016/j.soildyn.2008.08.006

[17] Sukmak, P., Horpibulsuk, S., Chinkulkijniwat, A.: Strength development of cement-admixed clay under cyclic loading, Soils and Foundations, 53 (2013) 1, pp. 1–12, DOI: 10.1016/j.sandf.2012.12.001

[18] Kampala, K., Horpibulsuk, S., Chinkulkijniwat, A.: Mechanical properties of stabilized silty clay, Construction and Building Materials, 47 (2013), pp. 1084–1093, DOI: 10.1016/j.conbuildmat.2013.06.041

[19] Tang, Y., Zhou, X., Yang, J.: Dynamic response of tunnel structures subjected to moving loads, Journal of Sound and Vibration, 318 (2008) 1–2, pp. 142–156, DOI: 10.1016/j.jsv.2008.04.017

[20] Vadillo, E.G., Gómez, J.G., Santamaría, J.: Dynamic response of railway tracks, Journal of Sound and Vibration, 193 (1996) 1, pp. 85–103, DOI: 10.1006/jsvi.1996.0266

[21] Wong, R.C.K., Law, C.K., Tang, W.H.: Ground-borne vibration due to railway traffic, Tunnelling and Underground Space Technology, 21 (2006) 3–4, pp. 322–331, DOI: 10.1016/j.tust.2005.12.001

[22] Connolly, D., Kouroussis, G., Verlinden, O., Forde, M.: Modelling ground vibration from high-speed rail lines, Soil Dynamics and Earthquake Engineering, 48 (2013), pp. 175–191, DOI: 10.1016/j.soildyn.2012.12.012

[23] Hall, L.: Simulations and Analyses of Train-Induced Ground Vibrations, PhD Thesis, Royal Institute of Technology (KTH), Stockholm, Sweden, 2003.

[24] Kouroussis, G., Verlinden, O., Connolly, D.: Ground vibration induced by high-speed trains, Journal of Sound and Vibration, 329 (2011) 9, pp. 1387–1403, DOI: 10.1016/j.jsv.2009.11.016

[25] Land Transport Authority: High-Speed Rail Design Code of China, Beijing, China

[26] American Association of State Highway and Transportation Officials (AASHTO): LRFD Bridge Design Specifications, 9th Ed., Washington, DC, USA, 2020.